A numerical study of the interaction between two ejecta in the interplanetary medium: one- and two-dimensional hydrodynamic simulations

A. Gonzalez-Esparza, A. Santillán, J. Ferrer

Annales Geophysicae (2004) 22: 3741–3749
SRef-ID: 1432-0576/ag/2004-22-3741

Annales Geophysicae

A numerical study of the interaction between two ejecta in the interplanetary medium: one- and two-dimensional hydrodynamic simulations

A. Gonzalez-Esparza[1], **A. Santillán**[2], **and J. Ferrer**[3]

[1]Instituto de Geofísica, Universidad Nacional Autónoma de México, Mexico City, Mexico
[2]Cómputo Aplicado-DGSCA, Universidad Nacional Autónoma de México, Mexico City, Mexico
[3]Facultad de Ciencias, Universidad Nacional Autónoma de México, Mexico City, Mexico

Received: 28 April 2004 – Revised: 7 July 2004 – Accepted: 16 August 2004 – Published: 3 November 2004

Abstract. We studied the heliospheric evolution in one and two dimensions of the interaction between two ejecta-like disturbances beyond the critical point: a faster ejecta 2 overtaking a previously launched slower ejecta 1. The study is based on a hydrodynamic model using the ZEUS-3-D code. This model can be applied to those cases where the interaction occurs far away from the Sun and there is no merging (magnetic reconnection) between the two ejecta. The simulation shows that when the faster ejecta 2 overtakes ejecta 1 there is an interchange of momentum between the two ejecta, where the leading ejecta 1 accelerates and the tracking ejecta 2 decelerates. Both ejecta tend to arrive at 1 AU having similar speeds, but with the front of ejecta 1 propagating faster than the front of ejecta 2. The momentum is transferred from ejecta 2 to ejecta 1 when the shock initially driven by ejecta 2 passes through ejecta 1. Eventually the two shock waves driven by the two ejecta merge together into a single stronger shock. The 2-D simulation shows that the evolution of the interaction can be very complex and there are very different signatures of the same event at different viewing angles; however, the transferring of momentum between the two ejecta follows the same physical mechanism described above. These results are in qualitative agreement with in-situ plasma observations of "multiple magnetic clouds" detected at 1 AU.

Key words. Interplanetary physics (flare and stream dynamics; interplanetary shocks; solar wind plasma)

1 Introduction

Coronal mass ejections (CMEs) are one of the most fascinating and energetic manifestations of solar activity, where a mass of about $10^{15}-10^{16}$ g is propelled out with a speed between $100-2000$ km/s, resulting with a kinetic energy around $10^{30}-10^{31}$ ergs (Hundhausen, 1999). Gopalswamy et al. (2001, 2002) reported the interaction between two CMEs close to the Sun: at the same time that the LASCO-SOHO observations showed a fast CME overtaking a previously launched slow CME, there was a radio signature in the form of an intense continuum-like radio emission following a type II interplanetary burst. Burlaga et al. (2001) studied the properties of fast ejecta detected at 1 AU by ACE spacecraft during a period of increasing solar activity and found "complex ejecta". These events are characterized by having disordered magnetic fields, high proton temperatures and long durations (about 3 days in ACE observations). They found that some of the complex ejecta in their study could have been produced by the interaction and merging of two or more CMEs in the interplanetary medium and these CMEs can be associated with a single source region. Recently, Odstrcil et al. (2003) used a 2.5 MHD model to investigate the interaction between two flux ropes in a homogeneous magnetized plasma. Their initial condition was one cloud and its shock wave in motion and the other cloud was at rest. They found that when the two clouds approached each other, their opposite magnetic fields were pushed together driving a magnetic reconnection (by numerical diffusion) and the two flux ropes gradually coalescence into a single flux rope.

However, not necessarily all overtaking CMEs in the interplanetary medium involve magnetic reconnection and form complex ejecta. Wang et al. (2003) reported three events of "multiple magnetic clouds", consisting of several magnetic clouds (MCs) separated by interacting regions. In these events, there was not a merging of the MCs in the interplanetary medium, and the successive halo CMEs associated with these clouds were not originated from a single source region. Figure 1 presents one of the events reported by Wang et al. (2003) showing ACE plasma observations of 3 magnetic clouds and 3 shock waves. Note that the interacting MCs are separated by plasma sheet signatures.

Similar intervals of a few days of in-situ spacecraft observations with a high number of ejecta and interplanetary shocks (no necessarily complex ejecta) appear in the literature. Some examples of these intervals are: the

Correspondence to: A. Gonzalez-Esparza
(americo@geofisica.unam.mx)

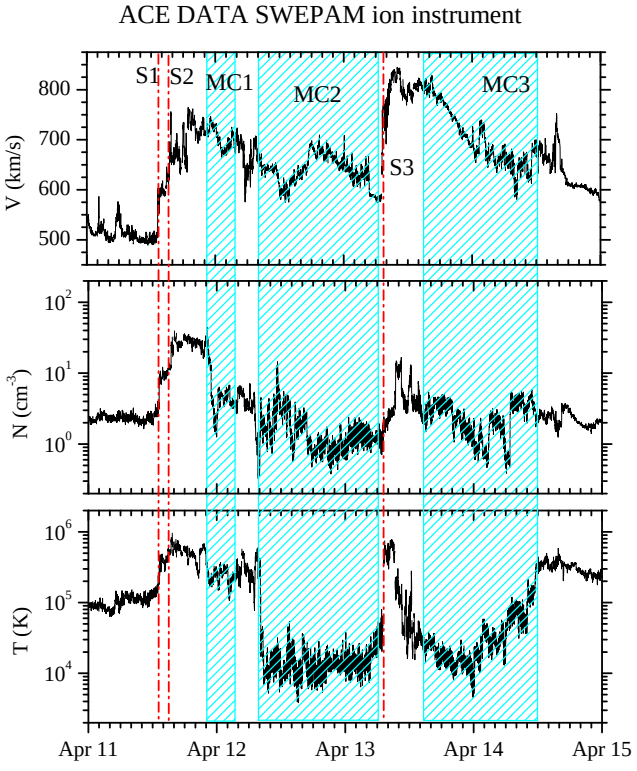

Fig. 1. Solar wind plasma observations of "multiple magnetic clouds" reported by Wang et al. (2003). The interval shows the interaction of three magnetic clouds and three interplanetary shock waves (data taken from the ACE SWEPAM (http://swepam.lanl.gov/).

August 1972 events detected by Pioneer 10 (Gonzalez-Esparza and Smith, 1996), the April 1979 events detected by Helios 2 (Berdichevsky et al., 2003), the March 1991 events detected by Ulysses (Phillips et al., 1992; Gonzalez-Esparza et al., 1996) and the April 2001 events detected by WIND (Berdichevsky et al., 2003). During these intervals the in-situ observations show a complex transferring of momentum between several ejecta and interplanetary shocks.

The interaction of CMEs can occur very close to the Sun, as those events reported by Gopalswamy et al. (2001) or at further heliocentric distances even beyond 1 AU. The characteristics of this interaction would depend on the physical properties of the colliding CMEs (velocity, mass, magnetic field configuration, size, time of ignition, etc.) and the ambient wind characteristics. The physics involved in CMEs colliding and merging close to the Sun (Odstrcil et al., 2003; Vandas and Odstrcil, 2004) is different than other cases, where the interaction occurs at further heliocentric distances and there is no magnetic reconnection (Fig. 1). This paper studies the latter case, where the evolution is driven by the dynamic pressure term of the large-scale disturbances and the ambient wind.

Based on a simple hydrodynamic model we present numerical simulations of the interaction between two ejecta-like disturbances and their associated shocks in the interplanetary medium to illuminate some physical aspects of their evolution in the inner heliosphere. The outline of the paper is as follows. Section 2 shows the characteristics of the numerical model and the initial conditions. Section 3 presents a numerical simulation in one dimension (1-D) which shows how the momentum is transferred from the trailing faster ejecta to the leading slower ejecta and the merging of their associated shocks into a stronger shock. This example shows how the interaction between the two ejecta affects their dynamic properties (velocity, radial width and transit time) as they propagate to 1 AU. Section 4 presents a simulation in two dimensions (2-D) showing the importance and complexity of the geometry in the interaction between the two ejecta. This 2-D simulation shows how different observers of the same event located at different heliographic longitudes detect very different signatures. Finally, Sect. 5 presents our conclusions.

2 Numerical simulations

We performed our study employing the numerical code ZEUS-3-D (version 4.2). This code solves the system of ideal MHD equations (non-resistive, non-viscous) by finite differences on an Eulerian mesh (Stone and Norman, 1992). In order to simplify the calculations we neglected all magnetic effects. Note here that beyond the critical point (18 solar radii) the solar wind becomes highly supersonic and the large-scale dynamics of the heliosphere is dominated by the dynamic pressure term of the solar wind streams. For this reason these simplified 1-D and 2-D hydrodynamic numerical simulations of interplanetary disturbances have proved to be very useful in understanding the basic physical aspects of the injection and heliospheric evolution of these disturbances (Hundhausen and Gentry, 1969; Dryer, 1994; Gosling and Riley, 1996; Riley et al., 1997, 2001; Gonzalez-Esparza et al., 2003a,b). However, we should keep in mind that there are fundamental issues that cannot be addressed by a hydrodynamic model. The model does not pretend to study the initiation of CMEs at the solar surface, nor the evolution of the topology of a magnetic cloud in the interplanetary medium, nor the complex plasma signatures shown in the in-situ measurements by spacecraft (e.g. alpha particles, bidirectional suprathermal electrons, heavy ions, etc.). Furthermore, the model cannot calculate the effects due to the magnetic reconnection that presumably occurs during the interaction and merging of some CMEs in the interplanetary medium. Therefore, we used this simplified model to study the interchange of momentum between large-scale interplanetary disturbances and solar wind streams driven basically by their dynamic pressures and interplanetary shocks, which play a predominant role in the large-scale dynamics of the solar wind.

Following a technique similar to that of Gosling and Riley (1996), we produced the ambient solar wind by specifying the fluid speed, density and temperature at an inner boundary located beyond the critical point (Ro=18 so-

lar radii=0.083 AU), and then allowing the wind to evolve and reach a stationary solution that mimics observed values of the solar wind at 1 AU. After the ambient solar wind was established, we injected a ejecta-like perturbation from the inner boundary to simulate the propagation of an ejecta into the interplanetary medium. These ejecta-like perturbations are pulses with an initial velocity and small increments in density and temperature, over a finite interval of time (τ_e). We include the solar gravity and assume that the solar wind is an ideal fluid with a ratio of specific heats, γ=1.5. All numerical runs have an in-flow condition at the inner boundary and an out-flow condition at the outer boundary (more details of these simulations can be found in González-Esparza et al. (2003a,b)).

Table 1. Characteristics of the ambient solar wind. Initial conditions at the inner boundary (Ro=0.083 AU) and stationary solutions at 1 AU in one and two dimensions.

	Ro	1.0 AU	
		1-D	2-D
N [cm^{-3}]	990	6.4	6.1
T [10^{5}K]	4.5	0.49	0.48
V [km/s]	400	426	447

Table 1 shows the initial conditions at the inner boundary to produce the ambient wind and the values of the stationary solution at 1 AU obtained by the 1-D and 2-D simulations. Note that the stationary solutions for the ambient wind had some small differences: the wind in the 1-D simulation tended to be sightly denser, hotter and slower than the one in the 2-D simulation. This discrepancy is because the 1-D simulation had a computational grid of 2048 zones with a resolution of 6.43e^{-4} AU per zone; whereas the 2-D simulation had a grid of 512×512 zones (spherical coordinates) with a resolution of 2.57×10^{-3} AU per radial zone and 6.13×10^{-5} radians per longitudinal zone.

3 One-dimensional simulation

After reaching the stationary solution for the ambient wind (V_{sw}=400 km/s) we injected during 5 h a slightly faster ejecta 1 (V_{e1}=450 km/s) and, 15 h after this initiation, we injected during 6 h a much faster ejecta 2 (V_{e2}=800 km/s). Table 2 shows the characteristics of the two ejecta-like pulses. These ejecta initial conditions are common values inferred from analyzing SOHO-LASCO movies and, in general, they are in good agreement with in-situ spacecraft measurements at 1 AU (Gonzalez-Esparza et al., 2003b).

In this case, the pulses representing ejecta-like perturbations had a initial square jump in velocity and, after half of the pulse duration, the velocity gradually decreased using a sinusoidal function toward the ambient wind value. This gradual decrement of the ejecta tail velocity is an artifice for diminishing the rarefaction region appearing at the back of a square pulse which produces an excessively strong reverse shock in the hydrodynamic simulation. From Table 2 we note that the total mass of ejecta 2 was about 2.1 times higher than the mass of ejecta 1, and the total kinetic energy of ejecta 2 was about 6.7 times higher than the energy in ejecta 1.

Figure 2 shows the heliocentric evolution of the two ejecta and their associated shocks propagating in the solar wind at three different times. Since the code has a numerical subroutine that tracks the leading and trailing edges of the two ejecta-like pulses at every time step, the plots show the radial extension of both ejecta as they propagate in the interplanetary medium. The plots at the left column in Fig. 2 shows the event at 20 h after ejecta 1 initiation, where the front of ejecta 1 is at R_{e1}=0.30 AU whereas ejecta 2 (R_{e2}=0.16 AU) is still is being injected. Both ejecta are driving a forward shock (s1 and s2) but clearly the front of ejecta 2 is much faster than the front of ejecta 1 and s2 is stronger than s1. At 40 h after ejecta 1 initiation, ejecta 2 (R_{e2}=0.46 AU) is very close to ejecta 1 (R_{e1}=0.52 AU) and s2 is propagating through ejecta 1. Note that as conforming s2 propagates, it is compressing and transferring momentum to ejecta 1, and the velocity of the tail of ejecta 1 is already of the same magnitude as the velocity of the front of ejecta 2. Finally, at 70 h after ejecta 1 initiation, the front of ejecta 1 (R_{e1}=0.91 AU) is already propagating faster than ejecta 2 (R_{e2}=0.88 AU), and s2 has already crossed ejecta 1 and has overtaken s1. The two forward shocks (s1 and s2) merge together into a stronger single shock.

Figure 3 shows the time evolution of the velocities of the front of ejecta 1 and ejecta 2 and the velocities of their associated shocks (s1 and s2). At the top of Fig. 3 the front of ejecta 1 propagates basically with a constant speed (V_{e1}=441 km/s) until at about 46 h (R_{e1}=0.58 AU), when it is overtaken by s2 and suffers an abrupt acceleration, thereby becoming faster (V_{e1}=591 km/s). The dotted curve in the same plot shows the velocity evolution of ejecta 1 for the case when there is no interaction with any other disturbance. In this case, there is no strong variation during its evolution but a gradual velocity decrement toward the ambient wind value due to the upstream wind dragging force. In the middle panel of Fig. 3, the front of ejecta 2 follows a very similar evolution as a single ejecta in the inner heliosphere: after its injection (V_{e2}=800 km/s) it reaches an intermediate speed (V_{e2}=630 km/s) with respect to the ambient wind and propagates with this quasi-constant speed until it reaches a critical point (R_{e2}=0.40 AU, t=29 h) from which it begins to decelerate. This critical point depends on the ejecta initial conditions and the ambient wind characteristics (Gonzalez-Esparza et al., 2003c). This plot shows that the velocity evolution of ejecta 2 is not affected significantly by ejecta 1. The plot at the bottom of Fig. 3 shows the velocity evolution of the two shock waves (s1 and s2) and their coalescing at 62 h into a stronger shock. Before this coalescing, s1 propagates with quasi-constant speed, whereas s2 is decelerating, thereby suffering some velocity fluctuations produced by its propagation against an upstream wind disturbed previously by s1 and ejecta 1.

Table 2. One-dimensional simulation. Characteristics of the ejecta-like pulses: Initial velocity (U_e), increment of density ($\Delta N_e = N_e/N_o$) and temperature ($\Delta T_e = T_e/T_o$) with respect to the ambient wind at ro, temporal duration (τ_e), total mass ($M_e = \sum_{i=1}^{n} mp \cdot N(r_i) \cdot d\vartheta(r_i)$) and total kinetic energy $\left(K_e = \sum_{i=1}^{n} (1/2) M_e(r_i) \cdot V^2(r_i)\right)$.

	V_e [km/s]	ΔT_e	ΔN_e	τ_e [h]	$M_e[10^{16}$g]	$K_e[10^{31}$ergs]
ejecta 1	450	1.2	1.2	5.0	3.1	3.14
ejecta 2	800	1.2	1.2	6.0	6.6	21.1

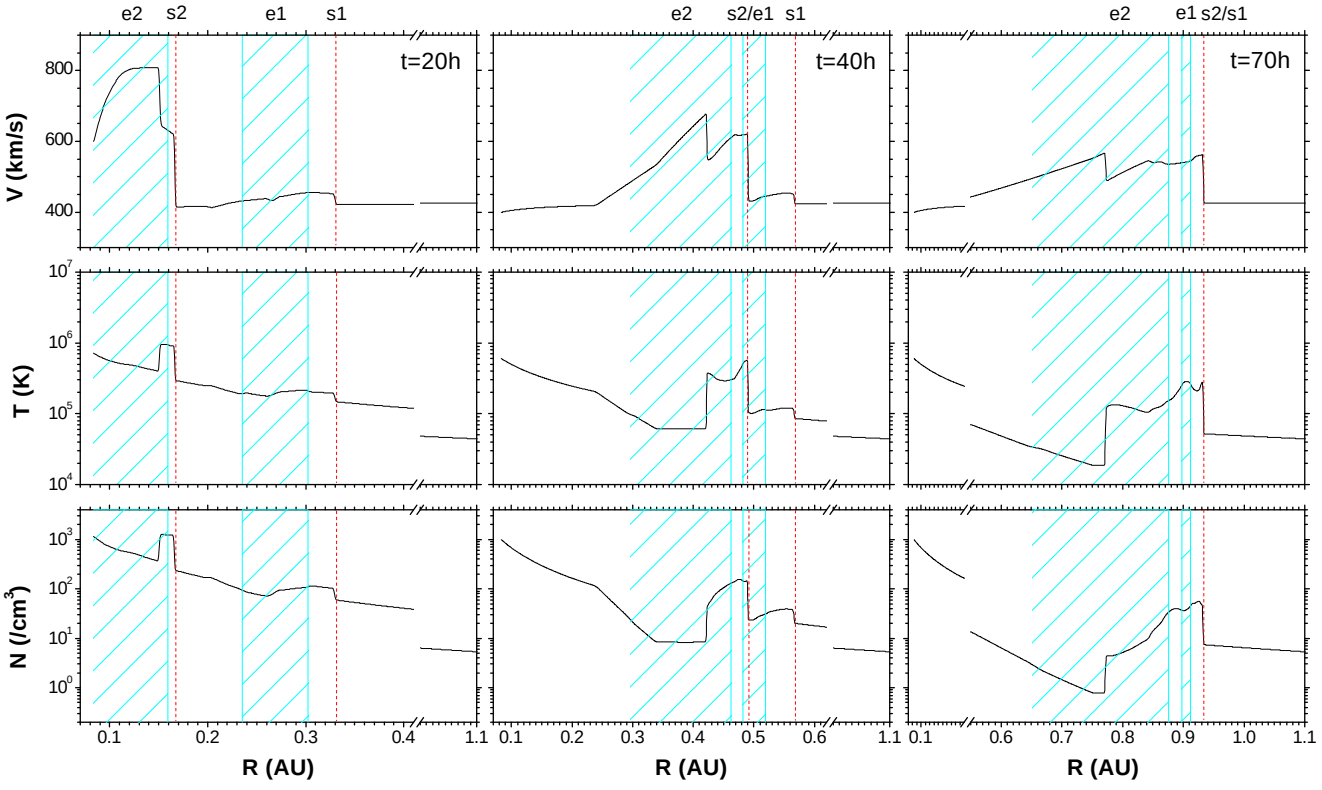

Fig. 2. Heliocentric evolution of two ejecta propagating in the solar wind at three different times after ejecta 1 initiation. The cases show the location of the two ejecta (e1, e2) and the vertical lines their shock waves (s1, s2). The scales on the horizontal axes were modified for each time to focus on the disturbances.

Figure 4 shows the evolution of the ejecta 1 radial width, which is injected during five hours and afterward it follows a gradual expansion until at about 32 h when it is compressed by the passing of the shock wave (s2) driven by ejecta 2. The dotted curve in the figure shows how ejecta 1 expands when there is not interaction with s2. The compression of ejecta 1 begins when s2 crosses by its tail and ends when s2 passes by its front, producing the abrupt acceleration shown at the top panel of Fig. 3. Keep in mind that this compression is overestimated by the model due to the lack of magnetic pressure into ejecta 1.

Figure 5 shows the evolution of the total kinetic energy of each ejecta (K_e), i.e. the sum of the kinetic energy of the cells covered by the ejecta. The top panel of Fig. 5 shows how the passing during 14 h of s2 through ejecta 1 increases the kinetic energy of the ejecta, showing clearly that the transferring of momentum between the two ejecta-like disturbances is basically by the interaction with the shock wave (s2). As it is shown in the same plot, if ejecta 1 is not compressed by s2, its total kinetic energy remains practically constant. At the bottom panel of Fig. 4, the kinetic energy of ejecta 2 decreases gradually with heliocentric distance (transferring momentum to the ambient wind) and, as in Fig. 3, the evolution of ejecta 2 looks very similar to the case when there is no interaction with any other disturbance.

Table 3 shows results at 1 AU of the 1-D simulation. For comparison columns 4 and 5 show the results obtained by the model when ejecta 1 and 2, respectively, propagate alone

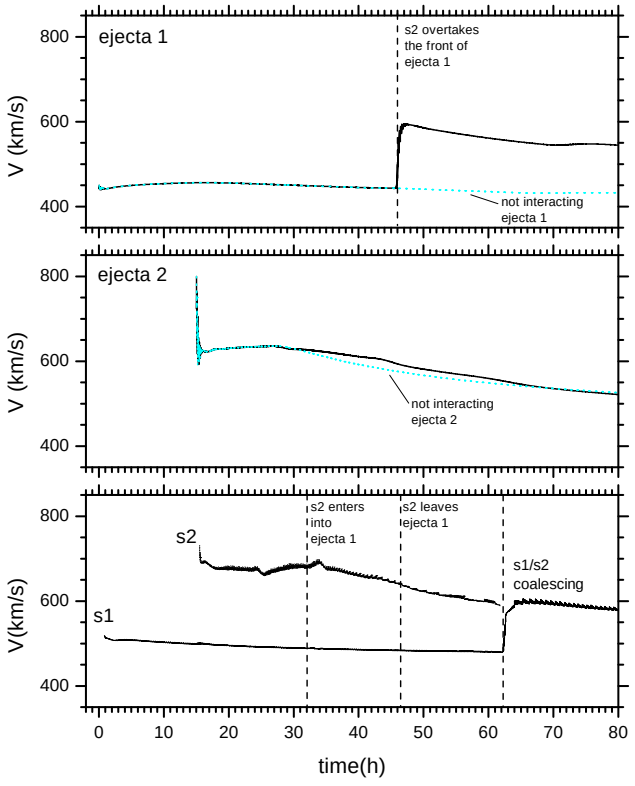

Fig. 3. Evolution of the velocities of the front of ejecta 1 (top), ejecta 2 (middle) and their associated shock waves (bottom). Ejecta 2 is injected 15 h after ejecta 1 initiation. The dotted curve in the top and middle plots show the evolution when there was no interaction with any other ejecta.

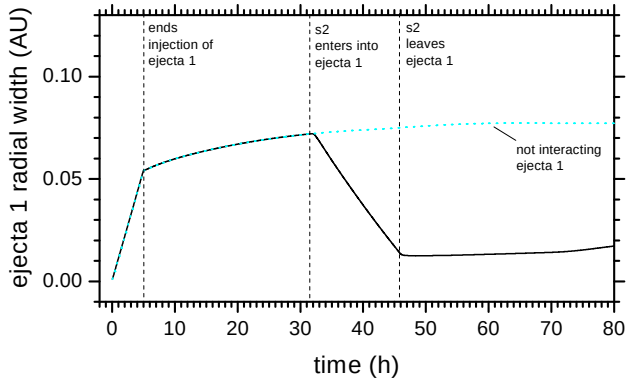

Fig. 4. Heliocentric evolution of the radial width of ejecta 1 (distance between its front and tail). The dotted curve shows the continuous expansion when there is no interaction with other disturbance.

against the ambient wind without interacting with any other disturbance. Although ejecta 1 was injected with a lower speed than ejecta 2, columns 2 and 3 show that at 1 AU their fronts arrived at 1 AU with similar speeds and moreover the front of ejecta 1 was faster. Note that the results of ejecta 2 were practically the same in columns 3 and 5, indicating that the interaction with ejecta 1 did not greatly affect

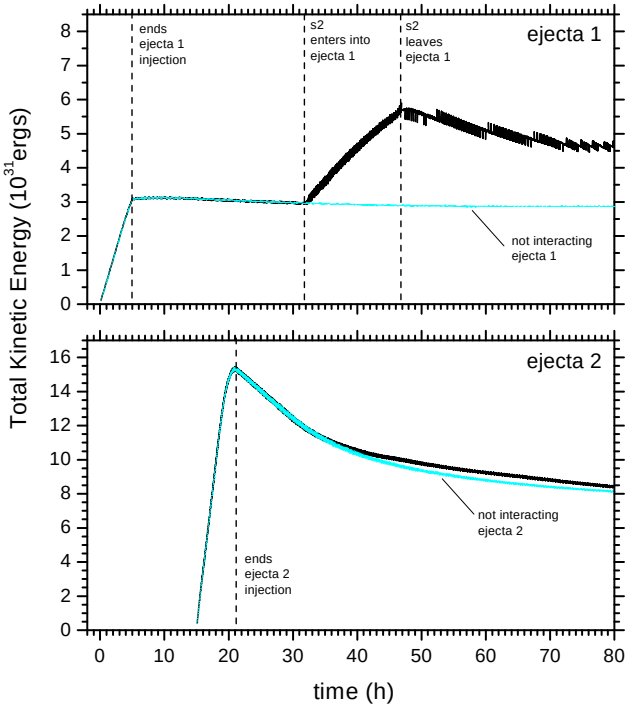

Fig. 5. Heliocentric evolution of the total kinetic energy of ejecta 1 (top) and ejecta 2 (bottom) $\left(K_e = (m_p/2) \cdot \sum_{i=1}^{n} V^2(r_i) \cdot N(r_i) \cdot d\vartheta(r_i)\right)$. The dotted curve in both plots shows the evolution when there was no interaction with other disturbance.

Table 3. One-dimensional results at 1 AU: ejecta transit time from ro ($\Delta t_{1\,AU}$), ejecta front velocity (V_e) and radial width (Wr_e). ($*$) ejecta propagates without interacting with other disturbance.

	ejecta1	ejecta2	ejecta1*	ejecta2*
$\Delta t_{1\,AU}$ [h]	76.6	64.7	85.6*	65.5*
V_e [km/s]	547	522	432*	525*
Wr_e [AU]	.016	.232	.077*	.223*

its propagation (the normalized differences between the two columns are less than 0.5%). However, the results of ejecta 1 in columns 2 and 4 were very different: due to the interaction with the shock wave driven by ejecta 2, ejecta 1 arrived at 1 AU compressed (with an approximate 79% smaller radial width) and with a much faster front speed (about 27% higher) and shorter transit time (about 10.5% less). These results agree with those by Vandas et al. (1997), where they studied the interaction of a shock wave overtaking a magnetic cloud (MC) using a MHD model. They found that the passing of the shock through the MC produces an increment in the MC's field magnitude and the ejecta is compressed and accelerated in the radial direction. This simulation explains why in three events reported by Wang et al. (2003) (Fig. 1), the front speed is faster in MC1 than in MC2, and the radial width is larger in MC2 than in MC1.

Table 4. Two-dimensional simulation. Characteristics of the ejecta-like pulses: initial velocity, increment of density and temperature, temporal duration, total mass and total kinetic energy as defined in Table 2.

	U_e [km/s]	ΔT_e	ΔN_e	τ_e [h]	$M_e[10^{16}\mathrm{g}]$	$K_e[10^{31}\mathrm{ergs}]$
ejecta 1	600	1.2	1.2	4.0	0.51	0.92
ejecta 2	1600	1.2	1.2	4.0	2.86	36.6

Table 5. Results in 2-D at the five radial cuts (a−e) at 57 h after ejecta 1 initiation (Fig. 7): ejecta heliocentric distance (R_e), ejecta front velocity (V_e) and ejecta radial width (Wr_e).

	ejecta 1			ejecta 2		
	e	d	c	c	b	a
R_e [AU]	0.79	0.95	1.08	1.04	1.02	0.97
V_e [km/s]	482	672	792	775	758	700
Wr_e [AU]	0.07	0.04	0.01	0.47	0.45	0.45

4 Two-dimensional simulation

The dynamics in the interplanetary medium of a shock wave and its driver has important 2-D and 3-D effects such as: there are tangential fluxes, the ejecta evolves toward a "pancake-like" shape (having larger longitudinal and latitudinal extents than the radial one), the shock has a larger angular range than its ejecta driver, the shock strength varies along the shock front, the shock-ejecta separation is different at the shock wings than at the shock nose, etc. (Odstrcil and Pizzo, 1999; Odstrcil, 2003). Therefore, the 1-D results shown in the previous section are limited to a simplified case where the observer is located at the passing of the nose of the IP shocks and the two ejecta coming afterward. In this section we present a numerical simulation in two dimensions to study some of these effects in the transferring of momentum between the two ejecta.

Table 4 shows the characteristics of the two ejecta-like pulses in the 2-D simulation. In this case the speed difference between the two ejecta is larger than in the previous section. Ejecta 1 was injected during 4 h at an angle of 51° with respect to the horizontal axis and having an angular extent of about 56°. At 15 h after this initiation, ejecta 2 was injected during 4 h at an angle of 91° with an angular extent of 70°. The total mass of ejecta 2 was about 5.6 times higher than the mass of ejecta 1, and the total kinetic energy of ejecta 2 was about 39.6 times higher than the energy of ejecta 1. Ejecta 2 was wider, massive and faster than ejecta 1.

Figures 6, 7 and 8 present snapshots of density contours (in color in the online version) showing the evolution of the simulation in 2-D at three different times. Denoted by characteristic curves over the contours we show the surfaces of the two ejecta (dotted lines) and the shock front (solid line). Associated with every snapshot there are five plots (a,b,c,d,e) with radial cuts at different angles: (a) is at the left wing of ejecta 2, (b) is at the center of ejecta 2, (c) is at the center of the interaction between ejecta 1 and ejecta 2, (d) is at the center of ejecta 1, and finally (e) is at the right wing of ejecta 1. In each plot we show the location of the ejecta (solid cases) and their shock waves (solid lines).

Figure 6 shows the simulation at 19 h after ejecta 1 initiation, where the front of ejecta 1 is propagating at about R=0.33 AU driving a shock wave (s1) and ejecta 2 has just been injected driving a stronger shock (s2). The five plots (a-e) show different features. In Figs. 6a,b there are only signatures of ejecta 2 and s2. In Fig. 6e only ejecta 1 and s1 are present. In Fig. 6d s2 propagates (without ejecta 2) behind ejecta 1, and in Fig. 6c the two ejecta propagate with their associated shocks (s1, s2).

Figure 7 shows the moment when ejecta 2 is overtaking ejecta 1 along the angular extent where they intersect at 29 h after ejecta 1 initiation. Here the effects of the tangential fluxes are important and the two ejecta become wider in their angular extents as they propagate outward. In Figs. 7a,b again there are only signatures of ejecta 2 and s2, but now these are different: the distance between the front of ejecta 2 and s2 is larger in Fig. 7b than in Fig. 7a, and the front of ejecta 2 propagates faster in Fig. 7b than in Fig. 7a. The plot 7c looks similar to the middle column of Fig. 2, where the two ejecta come very close to each other and s2 has already crossed through ejecta 1, compressing and accelerating the latter. In Fig. 7d, s2 is still propagating through ejecta 1 transferring momentum to ejecta 1, but there are no signatures of ejecta 2. Note that the trailing shock (s2) crosses ejecta 1 at different times at the different radial cuts, depending on the geometry and the characteristics of the event.

Figure 8 shows the event at 57 h after ejecta 1 initiation, at this time ejecta 2 is reaching 1 AU, whereas the right wing of ejecta 1 is still propagating in the inner heliosphere. In Figs. 8a,b the signatures of ejecta 2 and s2 present more differences: s2 is faster in Fig. 8b than in Fig. 8a, there is a strong reverse shock in Fig. 8b which does not appear in Fig. 8a, and the distance between the front of ejecta 2 and s2 is larger in Fig. 8b than in Fig. 8a. In Figs. 7c,d the two shocks had merged together and ejecta 1 is already propagating faster than the front of ejecta 2.

Table 5 summarizes some results of the two ejecta at the time of Fig. 8 along the five radial cuts (a−e). The two ejecta have different characteristics in each longitude. At (e) the front of the right wing of ejecta 1 is still propagating in the inner heliosphere (R=0.79 AU) with a speed of about

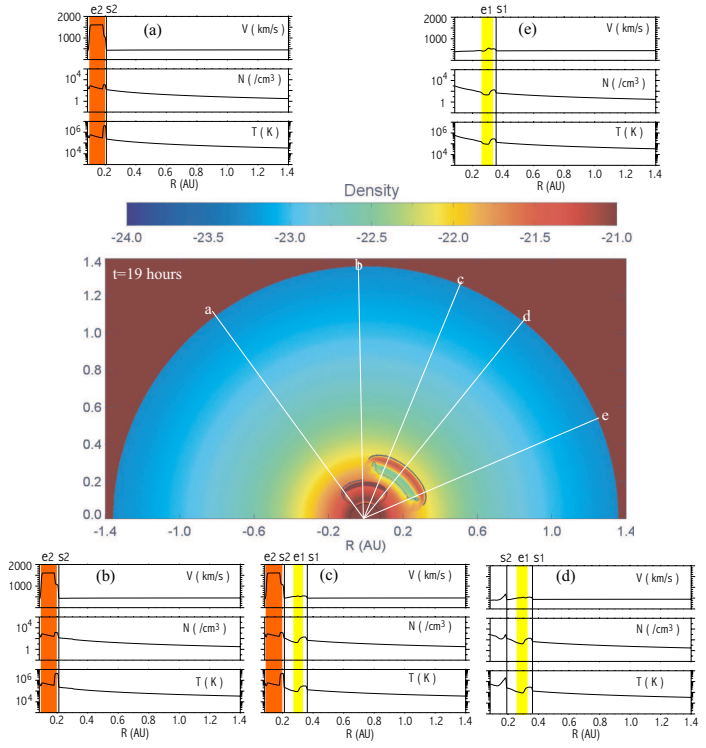

Fig. 6. Two-dimensional simulation. Snapshot of density logarithmic contours showing the evolution of the two ejecta at 19 h after ejecta 1 initiation. The five plots (**a**, **b**, **c**, **d**, **e**) show radial cuts of solar wind parameters at different angles denoting the ejecta (solid cases) and their shock waves (dotted lines).

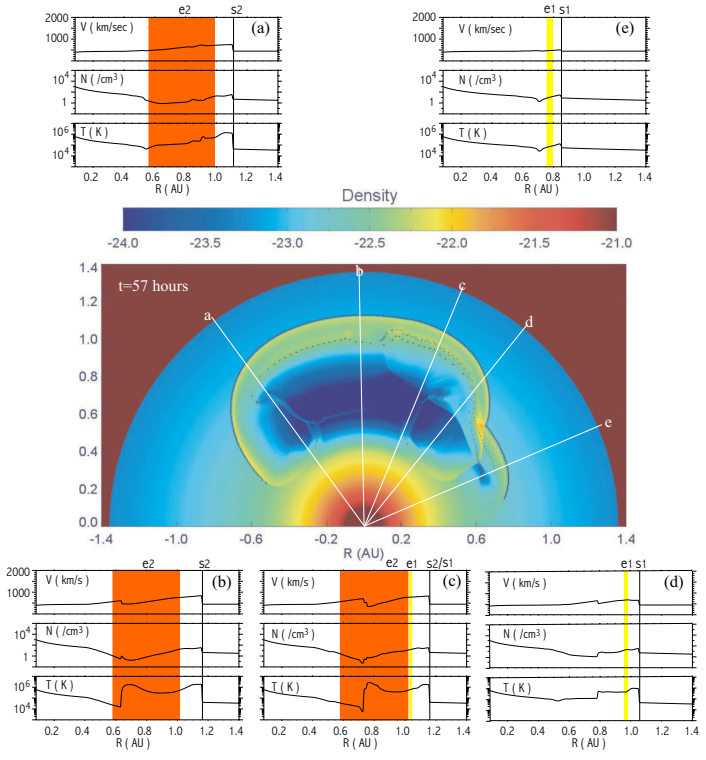

Fig. 7. Two-dimensional simulation. Snapshot of density logarithmic contours showing the evolution of the two ejecta at 29 h after ejecta 1 initiation. Same format as the previous figure.

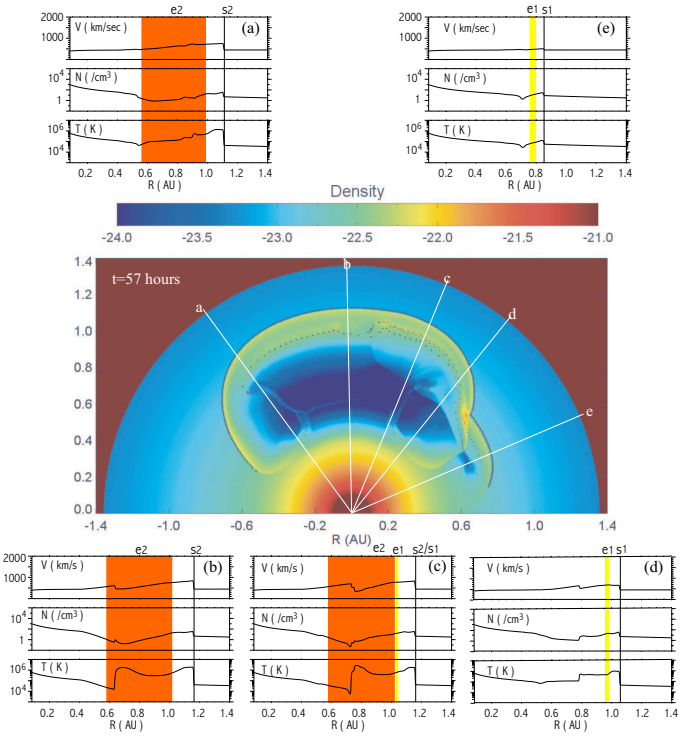

Fig. 8. Two-dimensional simulation. Snapshot of density logarithmic contours showing the evolution of the two ejecta at 57 h after ejecta 1 initiation. Same format as the previous figure.

V=482 km/s. At (c) ejecta 1 (R=1.08 AU) is already compressed and propagating faster than ejecta 2 (R=1.04 AU), and at (a) the left wing of ejecta 2 (R=0.97 AU) has a speed of about V=700 km/s.

The simulation shows that the evolution is more complex in two dimensions. Depending on the event characteristics at some angles there can be signatures only of a shock wave, or a shock and its ejecta, or an ejecta and two shocks, or two ejecta and two shocks, as has been shown in other simulations (Dryer, 1994; Riley et al., 1997; Odstrcil and Pizzo, 1999; Odstrcil, 2003). However, we found again that along the angular extension where both ejecta interact, eventually the initially slower ejecta 1 is compressed and its front becomes faster than the front of ejecta 2. The transferring of momentum between the two ejecta is mainly by the passing of the shock wave driven initially by ejecta 2 (s2) through ejecta 1. Note that this is also the case along the radial cut (d) in Figs. 6–8, where although there are no signatures of ejecta 2 driving s2 (the shock has always larger angular range than its driver), s2 compresses and accelerates ejecta 1.

5 Conclusions

The interaction between several shocks and ejecta in the interplanetary medium is a complex problem that has important implications for the propagation of large-scale solar wind disturbances and acceleration of solar energetic particles (SEPs) in the inner heliosphere (Vandas and Odstrcil, 2004). This interaction can occur on different scenarios depending on the characteristics of each event and not necessarily all the interacting CMEs merge and form complex ejecta. We performed two numerical exercises to study the interaction of two ejecta-like pulses beyond the critical point using a hydrodynamic model. As pointed out by Cargill and Schmidt (2002), hydrodynamic and MHD simulations of ejecta propagating in the interplanetary medium show similar evolutions of plasma structures, so we can apply a hydrodynamic model in those cases where the magnetic field effects are not dominant (e.g. there is no magnetic reconnection). The simulations show the transferal of momentum from ejecta 2 to ejecta 1. This momentum is transferred by the shock wave (s2) driven by the ejecta 2 which compresses and accelerates ejecta 1. Although the two ejecta were launched with disparate velocities, in the end they tend to arrive at 1 AU having similar speeds and the front of ejecta 1 ends propagating slightly faster than the front of ejecta 2. These results for the ejecta velocities and radial widths are in agreement with the plasma signatures of interacting MCs at 1 AU (Wang et al., 2003). Eventually, the two interplanetary shock waves driven by the two ejecta merge together into a single stronger shock.

Acknowledgements. We are grateful to X. Blanco-Cano and S. Kurtz for reading the early version of the manuscript. We are also grateful to P. Riley for providing the trace subroutine and the two referees for useful suggestions. We acknowledge the use of the data from the SWEPAM ion instrument on-board ACE spacecraft. This project was partially supported by CONACyT project J33127-E.

Topical Editor R. Forsyth thanks two referees for their help in evaluating this paper.

References

Berdichevsky, D. B., Farrugia, C. J., Lepping, R. P., Richradson, I. G., Galvin, A. B., Schwenn, R., Reames, D. V., Ogilvie, K. W., and Kaiser, M. L.: Solar-heliospheric-magnetospheric observations on 23 March−26 April 2001: Similarities to observations in April 1979, In M. Velli, editors, Solar Wind 10, AIP Conference proceedings, Woodbury, New York, 758–761, 2003.

Burlaga, L. F., Skoug, R. M., Smith, C. W., Webb, D. F., Zurbuchen, T. H., and Reinard, A.: Fast ejecta during the ascending phase of solar cycle 23 ACE observations, 1998–1999, J. Geophys. Res., 106, 20 957–20 977, 2001.

Cargill P. J. and Schmidt, S. M.: Medellin interplanetary CMEs using magnetohydrodynamic simulations, Ann. Geophys., 20, 879–890, 2002.

Dryer, M.: Interplanetary studies: propagation of disturbances between the sun and the magnetosphere, Space Sci. Rev., 67, 363, 1994.

Gonzalez-Esparza, J. A., Balogh, A., Forsyth, R. J., Neugebauer, M., Smith, E. J., and Phillips, J. L.: Interplanetary shock waves and large-scale structures: Ulysses' observations in and out of the ecliptic plane, J. Geophys. Res., 101, 17 057–17 072, 1996.

Gonzalez-Esparza, J. A. and Smith, E. J.: Solar cycle dependence of large-scale solar wind dynamics: Pioneer, Voyager, and Ulysses from 1 to 6 AU, J. Geophys. Res., 101, 24 359–24 371, 1996.

Gonzalez-Esparza, J. A., Lara, A., Pérez-Tijerina, E., Santillán, A., and Gopalswamy, N.: A numerical study on the acceleration and transit times of coronal mass ejections in the interplanetary medium, J. Geophys. Res., 108, doi:10.1029/2001JA009186, 2003a.

Gonzalez-Esparza, J. A., Lara, A., Santillán, A., and Gopalswamy, N.: A numerical study on the evolution of CMEs and shocks in the interplanetary medium, In M. Velli, editors, Solar Wind 10, AIP Conference proceedings, Woodbury, New York, 206–209, 2003b.

Gonzalez-Esparza, J. A., Cantó, J., Lara, A., and González, R.: Propagation of CMEs in the interplanetary medium: numerical and analytical results, Adv. Space Res., 32, 513–518, 2003c.

Gopalswamy, N., Yashiro, S., Kaiser, M. L., Howard, R. A., and Bougeret, J.-L.: Radio signatures of coronal mass ejection interaction: coronal mass ejection cannibalism?, Astrophys. J., 548, L91–L94, 2001.

Gopalswamy, N., Yashiro, S., Kaiser, M. L., Howard, R. A., and Bougeret, J.-L.: Interplanetary radio emission due to interaction between two coronal mass ejections, Geophys. Res. Lett., 29, GL013606, 2002.

Gosling, J. T. and Riley, P.: The acceleration of slow coronal mass ejection in the high speed wind, Geophys. Res. Lett., 23, 2867, 1996.

Hundhausen, A. J.: An introduction in Coronal Mass Ejections, in N. Crooker, J. A. Joselyn and J. Feynman, ed., Geophysical Monograph Series, 99, 1999.

Hundhausen, A. J. and Gentry, R. A.: Numerical simulations of flare-generated disturbances, J. Geophys. Res., 74, 2908, 1969.

Odstrcil, D.: Modeling 3-D solar wind structure, Adv. Space Res., 32, 497–506, 2003.

Odstrcil, D., Vandas, M., Pizzo, V. J., and MacNeice, P.: Numerical simulations of interacting magnetic flux ropes, In M. Velli, editors, Solar Wind 10, AIP Conference proceedings, Woodbury, New York, 699–702, 2003.

Odstrcil, D. and Pizzo, V. J.: Three-dimensional propagation of CMEs in a structured solar wind flow: 1. CME launched within the streamer belt, J. Geophys. Res., 104, 483–492, 1999.

Phillips, J. L., Bame, S. J., Gosling, J. T., McComas, D. J., Goldstein, B. E., Smith, E. J., Balogh, A., and Forsyth, R. J.: Ulysses plasma observations of coronal mass ejections, Geophys. Res. Lett., 19, 1239, 1992.

Riley, P., Gosling, J. T., and Pizzo, V. J.: A two-dimensional simulation of the radial and latitudinal evolution of a solar wind disturbance driven by a fast, high-pressure coronal mass ejection, J. Geophys. Res., 102, 14 677–14 686, 1997.

Riley, P.: CME dynamics in a structured solar wind, in Solar Wind Nine, ed. S. R. Habbal, R. Esser, J. V. Hollweg, and P. A. Isenberg, 131, AIP Conf. Proc., 471, Woodbury, NY, 1999.

Riley, P., Gosling, J. T., and Pizzo, V. J.: Investigation of the polytropic relationship between density and temperature within interplanetary coronal mass ejection using numerical simulations, J. Geophys. Res. 106, 8291, 2001.

Stone, J. M. and Norman, M.: ZEUS 2-D: A radiation magnetohydrodynamics code for astrophysical flows in two dimensions, I, the hydrodynamics algorithms and tests, Astrophys. J., 80, 753, 1992.

Vandas, M., Fischer, S., Dryer, M., Smith, Z., Detman, T., and Geranios, A.: MHD simulation of an interaction of a shock wave with a magnetic cloud, J. Geophys. Res., 102, 22 295–22 300, 1997.

Vandas, M. and Odstrcil, D.: Acceleration of electrons by interacting CMEs, Astronomy and Astrophysics, 415, 755–761, DOI:10.1051/00004-6361:20031763, 2004.

Wang, Y. M., Ye, P. Z., and Wang, S.: Multiple magnetic clouds: several examples during March−April 2001, J. Geophys. Res., 108, 1370, doi:10.1029/2003JA009850, 2003.